EEET ECOLOGICAL ENGINEERING & ENVIRONMENTAL TECHNOLOGY

Ecological Engineering & Environmental Technology, 2026, 27(6), 185–200
https://doi.org/10.12912/27197050/221535
ISSN 2719–7050, License CC-BY 4.0

Received: 2026.04.22
Accepted: 2026.05.18
Published: 2026.06.01

Controlled release of fenobucarb from polylactic acid core-shell nanofibers via coaxial electrospinning for sustainable pest control

Liem Thanh Nguyen[1*], Vu Anh Doan[1], Tuan Anh Phung[1], Phuong Nguyen Thi[1]

[1] School of Materials Science and Engineering, Hanoi University of Science and Technology, Hanoi, Vietnam
* Corresponding author's e-mail: liem.nguyenthanh@hust.edu.vn

ABSTRACT

This work reports a controlled-release pesticide platform based on fenobucarb-loaded core-shell nanofibers fabricated by coaxial electrospinning. Polylactic acid served as the biodegradable outer shell, while fenobucarb was incorporated into the inner core. The produced fibers had diameters ranging from 200 to 800 nm, with an average value of approximately 530 nm, and transmission electron microscopy confirmed the core-shell configuration. The loading content reached 17.976%, indicating effective incorporation of the active compound. Release experiments showed sustained fenobucarb release over a 30-day period, with an initial lag phase followed by a diffusion-driven process that was best described by the Higuchi model. Two formulation types, wettable powder and suspension concentrate, were developed and assessed on tomato crops under field conditions in Vietnam. In the preliminary field assessment, the suspension concentrate and wettable powder formulations showed descriptive efficacy values of 89.9% and 81.0% after 30 days, respectively, without visible phytotoxicity. Because the field assessment did not include replicated randomized plots, these values should be interpreted as preliminary evidence rather than statistically confirmed treatment superiority.

Keywords: fenobucarb, slow release, nanofiber, electrospinning, pesticide, polylactic acid

INTRODUCTION

During the 2023 to 2025 period, global pesticide expenditure is estimated at USD 80 to 90 billion, indicating continued reliance on chemical crop protection in intensive agriculture. These compounds remain essential for controlling pests and maintaining consistent food production (Majumder, 2024; Huang et al., 2025). Despite their importance, extensive use and poor application efficiency introduce significant environmental and health concerns. In typical conditions, less than one percent of the applied pesticide reaches the intended target (Elhamalawy et al., 2024; Liu et al., 2025). The majority disperses into the environment through volatilization, surface runoff, photodegradation, and leaching into soil and water. This inefficiency increases operational costs, promotes accumulation of toxic residues, and contributes to long term environmental pollution (Carvalho, 2017; Chawda et al., 2021).

Long-term and large-scale pesticide use has been associated with soil biodiversity loss, adverse effects on terrestrial and aquatic organisms, and contamination of surface and groundwater through runoff and leaching. These problems are more pronounced in developing regions, where misuse, excessive application, and limited regulatory oversight remain common. In Vietnam, intensive pesticide use has been linked to biodiversity loss, soil deterioration, and water pollution (Nguyen, 2018). Repeated application also promotes pest resistance, increasing chemical demand and raising concerns about the sustainability of current agricultural practices (Ahmad et al., 2024; Zhou et al., 2025). Conventional pesticide formulations also face technical limitations. Active ingredients can degrade under light, temperature, and moisture, reducing residual activity and requiring frequent reapplication. This increases production costs, pesticide input, and environmental pressure, highlighting the need for

more efficient controlled-release delivery systems (Alessandro et al., 2024; Hongling et al., 2026).

Nanotechnology offers a practical route to improve pesticide formulations by enhancing solubility, stability, bioavailability, and delivery efficiency of active ingredients. Several nanoformulation methods have been explored, including nanoprecipitation for polymer-based nanoparticles, emulsion methods for hydrophobic compounds, encapsulation systems such as polymeric carriers and liposomes, and scalable approaches such as spray drying and ionic gelation (Xin et al., 2020; Honghong et al., 2022). Nanopesticides use nanoscale carriers to improve pesticide performance through better dispersion, stronger interaction with target surfaces, and regulated release. Their high surface area can enhance contact with plant surfaces, while improved adhesion can reduce losses from rainfall or irrigation. These features help maintain more active ingredient at the target site and reduce off-target environmental loss (Rida et al., 2024; Huanyu et al., 2025).

A variety of nanocarrier systems have been developed, including polymeric nanoparticles, silica based materials, lipid carriers, and nanocapsules. These structures function as protective matrices that isolate active compounds from environmental stress. They reduce exposure to ultraviolet radiation, temperature fluctuations, and microbial degradation, which improves stability and extends effectiveness under field conditions (Zhao et al., 2023; Chen et al., 2021). These systems are designed to minimize premature degradation, enhance adhesion to plant surfaces, and regulate the release of active ingredients. Some carriers respond to external stimuli such as pH, light, or enzymatic activity, which allows more targeted and efficient delivery (Jun et al., 2025; Yu et al., 2023). Among available approaches, polymer based controlled release systems attract strong interest. In these systems, pesticides are embedded within biodegradable matrices and released gradually, which maintains effective concentrations and reduces the need for repeated application. Poly(lactic acid) is widely applied due to its biodegradability and compatibility with the environment (Oluwatoyin et al., 2025).

Electrospinning is a flexible technique for producing nanofiber-based controlled-release systems. It generates fibers with high surface-to-volume ratios, which support active ingredient loading and controlled diffusion. Coaxial electrospinning further enables the formation of core-shell fibers, where the active compound is enclosed within a polymer shell. This structure can improve stability, reduce wash-off, enhance plant surface retention, and prolong pesticide release (Doan et al., 2025; Gaydhane et al., 2023; Ananya et al., 2023). Fiber morphology and release behavior depend strongly on processing conditions, including applied voltage, flow rate, polymer concentration, temperature, and humidity. These parameters influence jet stability, solvent evaporation, fiber diameter, and structural uniformity, which ultimately affect loading efficiency and release performance (Kalluri et al., 2021; Raksa et al., 2021).

Coaxial electrospinning is an advanced form of electrospinning that uses a dual-channel nozzle to produce core-shell nanofibers. In this structure, the active compound is placed in the inner core, while the outer polymer shell acts as a protective barrier (Doan et al., 2025; Jahangir et al., 2024). The shell can protect the active ingredient from ultraviolet radiation, temperature changes, and moisture, while shell thickness, polymer composition, and core-to-shell ratio can be adjusted to control the release profile (Nguyen et al., 2026; Alli et al., 2024; Viter et al., 2025). Electrospun nanofibers also have high porosity and large surface-to-volume ratios, which improve plant surface contact, active ingredient loading, and controlled diffusion. These properties support gradual release, reduce pesticide loss, and limit off-target dispersion, making them suitable for prolonged agricultural applications (Nguyen et al., 2026; Khan et al., 2024; Le et al., 2024).

The combination of nanotechnology, biodegradable polymers, and advanced fabrication techniques provides a strong foundation for developing next generation pesticide delivery systems. These approaches improve application efficiency, lower environmental impact, and support sustainable agriculture. Several challenges remain, including issues with large scale production, high cost, regulatory constraints, and uncertainty regarding long term environmental safety. Further studies should focus on field evaluation and the development of standardized assessment methods for practical implementation (Kah et al., 2019; Wang et al., 2026).

Tomato plants (Solanum lycopersicum) are susceptible to aphid infestation, and fenobucarb is commonly used for aphid control. However, conventional fenobucarb formulations often

show limited residual activity and require repeated application. Although nanopesticides and controlled-release systems have been widely investigated, the use of coaxial electrospun PLA core-shell nanofibers for fenobucarb delivery and their conversion into practical agricultural formulations remain insufficiently demonstrated, especially under real field conditions.

Therefore, this study aimed to fabricate fenobucarb-loaded PLA core-shell nanofibers by coaxial electrospinning, characterize their morphology, loading content, and release behavior, and convert them into wettable powder and suspension concentrate formulations for preliminary field assessment against aphids on tomato crops. The specific objectives were: (i) to fabricate fenobucarb-loaded PLA core-shell nanofibers by coaxial electrospinning; (ii) to characterize their morphology, loading content, and release kinetics; (iii) to develop wettable powder and suspension concentrate formulations from the nanofibers; and (iv) to assess aphid control performance and phytotoxicity under tomato cultivation conditions. We hypothesized that the PLA shell would delay water penetration and fenobucarb diffusion, resulting in sustained release and extended aphid suppression compared with the commercial fenobucarb formulation, without causing visible phytotoxicity to tomato plants.

MATERIAL AND METHODS

Matrials

Polylactic acid (PLA, Resomer® R203H, Mw 18,000 to 24,000, density 1.24 g/cm³) was obtained from Sigma-Aldrich. Chloroform, N,N-dimethylformamide, and toluene were provided by Xilong Scientific Co., Ltd. and used as solvents. Fenobucarb (98%, density 1.46 g/cm³) was supplied by D&C Chemical Co., Ltd. The commercial product Dibacide 50 EC, containing 500 g/L fenobucarb, was obtained from Sara Co., Ltd. and used as a reference formulation.

Additional components for preparing the nano formulated pesticide products included tristyrylphenol ethoxylates (viscosity 920 cps), alkyl naphthalene sulfonate (39.2% with unsulfonated oil content below 1.25%), nano silica (99.7%, particle size 200 nm), sodium lignosulfonate (density 0.5 g/cm³), lauryl sodium sulphate (melting point 206 °C, water soluble), and the emulsifier Vanzan NF (viscosity 1400 to 1600 mPa·s, particle size 180 μm). Dry sand and kaolin were also used. All materials were sourced from Xilong Scientific Co., Ltd. and applied without further purification.

Preparation of CSNFs

To prepare the shell solution, 10 g of polylactic acid was dissolved in 90 mL of a chloroform and N,N-dimethylformamide mixture with a weight ratio of 90:10. The solution was stirred using a magnetic stirrer at approximately 40 °C until complete dissolution, resulting in a 10 wt.% polylactic acid solution. The core solution was prepared by dissolving fenobucarb (98%) in toluene to obtain a concentration of 10 wt.%.

To ensure the reproducibility of the study, the viscosities of the PLA and FNC solutions were measured using a Brookfield DV-E digital viscometer equipped with an LV-2 spindle at 100 rpm and 25 °C, following ASTM D2196. The reported viscosity of each solution was calculated as the average of five measurements. The electrical conductivities of the PLA and FNC solutions were measured at 25 °C using a conductivity meter (MeterLab CDM210, Radiometer Analytical, France). The physicochemical properties of the electrospinning solutions are presented in Table 1.

According to the instrument specification, the measurable conductivity range is 0.01 μS/cm to 400 mS/cm using a cell constant of 1 cm^{-1}. The electrical conductivity of the 10 wt.% fenobucarb solution in toluene was below the reliable quantification range under the applied measurement conditions and was therefore reported as below detection limit.

Core shell nanofibers were produced using coaxial electrospinning of the prepared solutions. After cooling to room temperature, both solutions were loaded into 5 mL syringes connected to a stainless steel coaxial spinneret with a 21 gauge needle.

Based on previously reported conditions, the electrospinning parameters were set as follows: shell and core flow rates of 0.6 and 0.18 mL/h, an applied voltage of 16 kV, and a distance of 18 cm between the needle tip and the collector.

During electrospinning, the jet behavior was monitored to assess process stability and reproducibility. The formation of a stable Taylor cone, continuity of the coaxial jet, jet interruption,

Table 1. The physicochemical properties of the electrospinning solutions

Solution	Concentration	Solvent system	Conductivity, μS/cm	Viscosity, mPa·s
PLA solution	10 wt.%	$CHCl_3$/DMF (90/10)	5.23	123.6
Fenobucarb solution	10 wt.%	Toluene	Below detection limit	42.3

dripping at the needle tip, bead formation, and visible jet fluctuation were observed throughout the process. Operating parameters, including applied voltage, shell flow rate, core flow rate, tip-to-collector distance, spinning time, temperature, and relative humidity, were recorded together with jet stability observations in an electrospinning log, as shown in Table 2

The process yield was calculated as the ratio between the dry mass of collected CSNFs and the theoretical total solid mass of PLA and fenobucarb introduced through the shell and core feed solutions. The batch-to-batch variation in process yield was approximately ±9%, mainly due to minor fluctuations in jet stability, solvent evaporation, fiber deposition efficiency, and mechanical losses during fiber mat collection. Small differences in solution homogeneity and actual feed delivery may also have contributed to this variation.

All experiments were carried out under ambient conditions at 25 °C and 50% relative humidity. The electrospinning process was continued for 2 h after stable jet formation to collect the nanofibers under steady spinning conditions. A schematic illustration of the coaxial electrospinning setup is shown in Figure 1.

Preparation of the nano pesticide fomulations from CSNFs

Two nano pesticide formulations, wettable powder (WP) and suspension concentrate (SC), were prepared using CSNFs as the active scaffold. In this system, fenobucarb is located in the core, while polylactic acid forms the outer protective layer. Both formulations were designed in compliance with the Vietnam National Standard. Each product was prepared using defined proportions of raw materials, including CSNFs

Table 2. Electrospinning operating log and jet stability observation

Parameter	Recorded value	Supporting evidence
Taylor cone formation	Stable	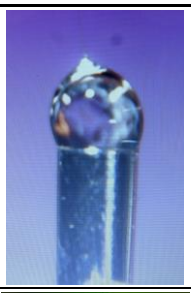
Coaxial jet continuity	Continuous	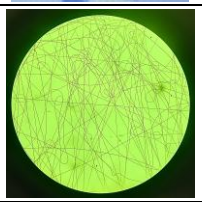
Jet interruption	Not observed	Visual observation
Visible jet fluctuation	Low	Visual observation
Collector condition	Uniform fiber deposition	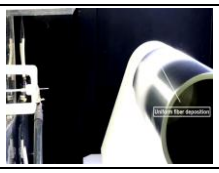
Process yield	83.1 ± 9%	Three batches

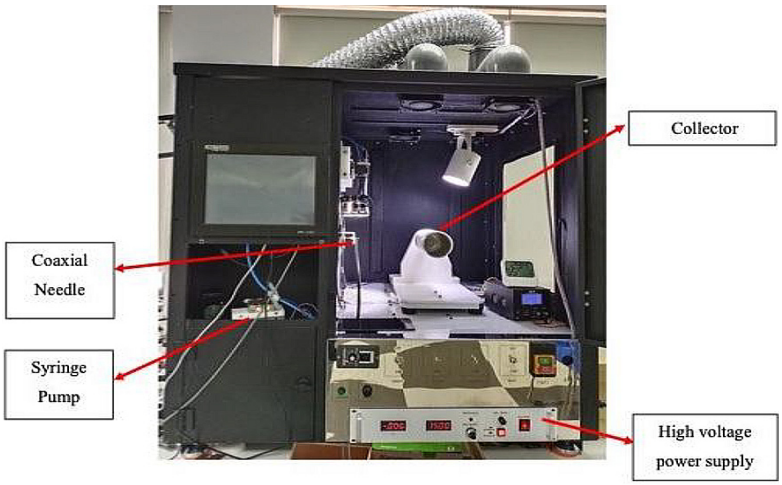

Figure 1. Schematic view of coaxial electrospinning process

containing encapsulated fenobucarb, as detailed in Table 3.

For the wettable powder formulation (WP), tristyrylphenol ethoxylates were used as the dispersing agent, alkyl naphthalene sulfonate as the surfactant, and nano silica as the anticaking additive. These components were first blended in a mechanical mixer for 5 minutes. CSNFs were then introduced, and mixing continued for an additional 15 minutes. The mixture was subsequently processed using a disc mill operating at 1500 rpm for 60 minutes to obtain particles with sizes below 10 µm.

For the suspension concentrate formulation (SC), CSNFs and sodium lignosulfonate were dispersed in water and premixed in a reactor at 600 rpm to form an initial suspension. Sodium lauryl sulphate was then added as a surfactant, and the system was stirred at 1000 rpm for 60 minutes. The dispersion was further milled to reach the desired particle size. After grinding, the suspending agent Vanzan NF was incorporated, followed by a final homogenization step carried out at approximately 1000 rpm for 2 hours.

Table 3. Fomulation recipe for nano pesticide products (WP and SC)

Ingredients	Weight ratio, %	
	WP	SC
CSNFs	30	30
Lauryl sodium sulphate	-	3
Tristyrylphenol ethoxylates	4	-
Alkyl naphthalene sulfonate	3	-
Sodium lignosulfonate	-	4
Vanzan NF	-	3
Nano silica	2	-
Kaolin	55	-
Dry sand	-	-
Water	6	60
Total	100	100

Characterization of CSNFs

The morphology of the core-shell nanofibers was characterized using scanning electron microscopy (SEM, JSM 6510LV, Japan). Before SEM observation, the electrospun nanofiber mats were carefully removed from the collector and cut into small pieces. Each sample was fixed onto an aluminum SEM stub using double-sided conductive carbon tape. The samples were then dried at room temperature to remove residual solvent and moisture. Before imaging, the samples were sputter-coated with a thin conductive layer of gold to reduce surface charging during SEM observation.

SEM images were taken from different areas of each sample to ensure representative observation of the fiber morphology. Fiber diameter was analyzed from SEM images using ImageJ software. For each sample, 100 fibers were randomly selected from different image regions to determine the average diameter and diameter distribution.

The internal structure of the fenobucarb/PLA core-shell nanofibers was examined using transmission electron microscopy (TEM, JEM-2100, JEOL, Japan) at an accelerating voltage of 200 kV. Samples were prepared by directly depositing electrospun fibers onto carbon-coated copper grids for approximately 5 s. The

prepared grids were then analyzed by TEM to visualize the core-shell structure. Because the electron beam must pass through the full fiber diameter, fibers with diameters below approximately 300 nm were selected to allow clear observation of the internal structure.

Determination of fenobucarb loading capacity

Fenobucarb loading and release were quantified using gas chromatography with a flame ionization detector (GC-6890N, Agilent, USA), with etofenprox used as an internal standard. Approximately 10 mg of fenobucarb/polylactic acid nanofibers were randomly collected and dissolved in 10 mL of chloropicrin using ultrasonic treatment until a homogeneous solution was obtained. The resulting solution was analyzed to determine fenobucarb content, as described in Equation 1.

$$Fenobucarb\ (\%) = \\ = \frac{mass\ of\ fenobucarb\ in\ CSNFs}{mass\ of\ dry\ CSNFs} \times 100 \quad (1)$$

In vitro fenobucarb release

The in vitro release behavior of fenobucarb/PLA core-shell fibers was evaluated by immersing the fiber specimens in deionized water under controlled conditions. Deionized water was selected as the release medium to represent aqueous environmental exposure under agricultural conditions.

Because fenobucarb has limited water solubility, fenobucarb released into the medium was extracted with an organic solvent before GC-FID analysis. Fiber specimens with a size of 1 × 1 cm and a mass of approximately 10 mg were randomly cut from the core-shell fiber membranes. Each specimen was placed in a sealed glass bottle containing 40 mL of deionized water. The bottles were maintained at approximately 40 °C for 30 days. Samples were collected at 1, 2, 3, 5, 7, 10, 15, 20, 25, and 30 days. After each sampling, the same volume of fresh deionized water was added to maintain a constant release volume. Before GC-FID quantification, fenobucarb in the collected aqueous medium was extracted using an organic solvent. The organic phase was collected, filtered through a 0.22 μm membrane filter, and analyzed using gas chromatography with a flame ionization detector (GC-FID). Fenobucarb concentrations were determined from a calibration curve prepared using standard fenobucarb solutions, with etofenprox used as the internal standard.

The cumulative amount of fenobucarb released from the fiber mats was calculated at each sampling time. The release percentage was expressed as the ratio between the amount of fenobucarb released at time t and the total amount of fenobucarb initially loaded in the core-shell fibers, as shown in Equation 2.

$$Release\ \%\ (t) = \frac{M_t}{M_n} \times 100 \quad (2)$$

In Equation 2, M_t (mg) represents the amount of fenobucarb released at a given time interval and M_n (mg) denote the total amount of fenobucarb initially encapsulated within the fenobucarb/polylactic acid CSNFs.

Mathematical models

To investigate the release mechanism of fenobucarb from fenobucarb/polylactic acid CSNFs, the experimental data were analyzed using different kinetic models, including zero order, Higuchi, and Korsmeyer Peppas models. For the zero-order model, the release rate constant (k) is obtained from the linear relationship between the amount released and time. In this case, the cumulative amount of fenobucarb released (M_t) increases proportionally with time, while the remaining concentration (C) decreases linearly from the initial concentration (C_0), as described in Equation 3.

$$Q_t = k_0 t + C \quad (3)$$

In the Higuchi model, the release constant (k) is derived from a diffusion controlled mechanism, where the cumulative amount of fenobucarb released (M_t) is proportional to the square root of time (t). This model assumes a homogeneous matrix system, in which the release behavior depends on the initial loading of the active ingredient (M_0), as described in Equation 4.

$$Q_t = k_H\, t^{1/2} + C \quad (4)$$

In the Korsmeyer Peppas model, both the release rate constant (k) and the diffusion exponent (n), referred to as the Korsmeyer Peppas parameter, are obtained from the relationship between the cumulative amount of fenobucarb released at time M_t and the initial loading M_0, as described in Equation 5.

$$\frac{M_t}{M_0} = kt^n \quad (5)$$

Preliminary field performance assessment

The field layout used for the preliminary assessment is illustrated in Figure 2. A small-scale field efficacy assessment was conducted in Tam Duong commune, Phu Tho province, Vietnam, to evaluate the practical performance of the developed formulations under tomato cultivation conditions. The assessment included four treatments: WP formulation, SC formulation, commercial Dibacide 50 EC, and an untreated control. Each treatment was applied to one plot with an area of 400 m². The plots were arranged sequentially, with a 1 m buffer zone between adjacent plots to reduce treatment interference. The entire experimental area was located at least 1 m away from the field boundaries.

Because this assessment was designed as an initial field screening trial, replicated randomized plots were not included. Therefore, the field data were used to describe treatment performance trends rather than to support inferential statistical comparison among treatments. Further replicated and randomized field trials are required to confirm the efficacy of the developed formulations and compare them statistically with commercial products.

The site was located at 21.21347° N and 105.36124° E, with an elevation of 25 m above sea level. This study was carried out from September 15, 2025 to October 16, 2025 to monitor pest and disease development, and continued until harvest in March 2026 to evaluate formulation performance. The experiment was conducted on tomato crops grown in raised beds at the leaf development stage. The soil type was sandy loam under a monoculture system. Fertilizer application per hectare per crop included 1000 kg of farmyard manure, 600 kg of lime, 150 kg of urea, and 150 kg of potassium sulfate.

On the application day, temperatures ranged from 26 to 30 °C under light sunshine. During the following period, weather conditions remained mostly sunny with no immediate rainfall. Rainfall events occurred at 3, 5, 6, and 10 days after application, with precipitation levels ranging from 15 to 35 mm per event. Throughout the assessment period, temperature ranged from 24 to 32 °C, while relative humidity ranged from 60% to 75%. Nematodes were observed at the site during the assessment period. This observation was recorded as a possible background field factor, but nematode effects were not evaluated in this study, while no other pest species were detected in the field.

Aphid density was recorded at ten sampling points within each plot. The sampling points were arranged along two diagonal transects, and each point was located at least 1 m from the plot boundary to reduce edge effects. Mean aphid density was calculated from these within plot observations and expressed as aphids per leaf. These sampling points were used to describe within plot variation and treatment trends, but they were not treated as independent field plot replicates for statistical comparison.

The descriptive efficacy of the treatments against aphid infestation was calculated using the Henderson-Tilton formula, which accounts for changes in aphid population density before and after treatment in both treated and untreated plots, as presented in Equation 6. Because the field assessment did not include replicated randomized

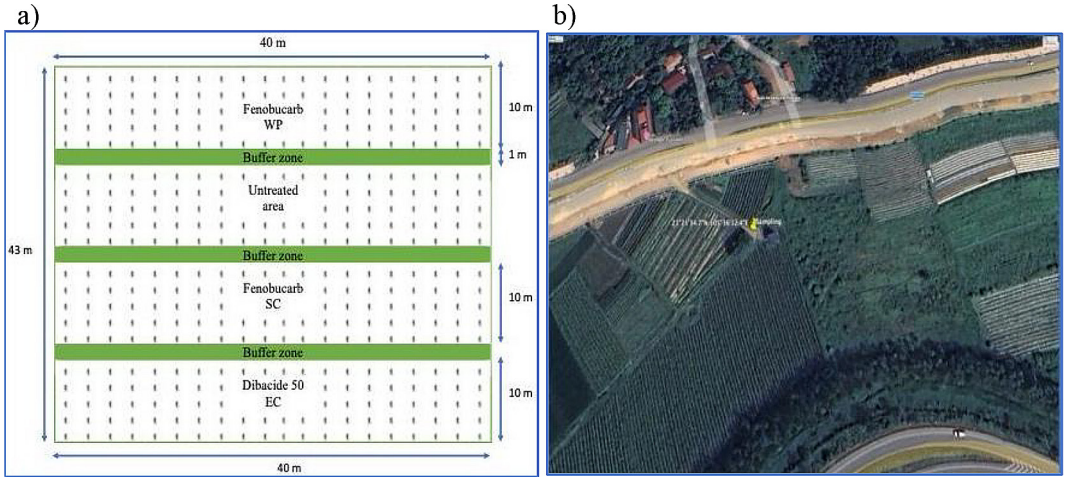

Figure 2. Field experiment block design (a), test location at Tam Duong commune, Phu Tho province, Vietnam (b)

plots, no inferential statistical analysis was performed for treatment comparison.

$$E\,(\%) = 1 - \frac{Ta \times C\,b}{Tb \times Ca} \times 100 \qquad (6)$$

where: E – effectiveness of the tested pesticide, (%); Ta, Tb – density of live aphids in the treated plot after, before treatment; Ca, Cb – density of live aphids in the control plot after, before treatment

Because individual sampling-point values were not retained, SD values were not calculated. The field data were therefore presented descriptively and were not used for inferential statistical comparison.

RESULTS AND DISCUSSION

Morphology of fenobucarb/polylactic acid CSNFs

The morphology of fenobucarb/polylactic acid CSNFs was characterized using scanning electron microscopy (SEM) and transmission electron microscopy (TEM), as illustrated in Figure 3. It shows that the fenobucarb/polylactic acid CSNFs possess relatively small fiber diameters with a narrow distribution. The diameters range from 200 to 800 nm, with an average value of 530 nm and a standard deviation of 79 nm (Figure 3c).

SEM observations (Figure 3b) reveal that the fibers do not exhibit a uniform size or shape. The presence of ribbon like, twisted, and non uniform structures is associated with the solvent system and polymer concentration used during coaxial electrospinning. The shell solution, consisting of chloroform ($CHCl_3$) and dimethylformamide (DMF), shows a clear difference in volatility. $CHCl_3$ evaporates rapidly, while DMF evaporates more slowly. This difference leads to early solidification of the outer layer, while residual solvent remains trapped inside the fiber. As the remaining solvent evaporates during flight or after deposition, the internal structure collapses, resulting in flattened and ribbon like fiber morphology.

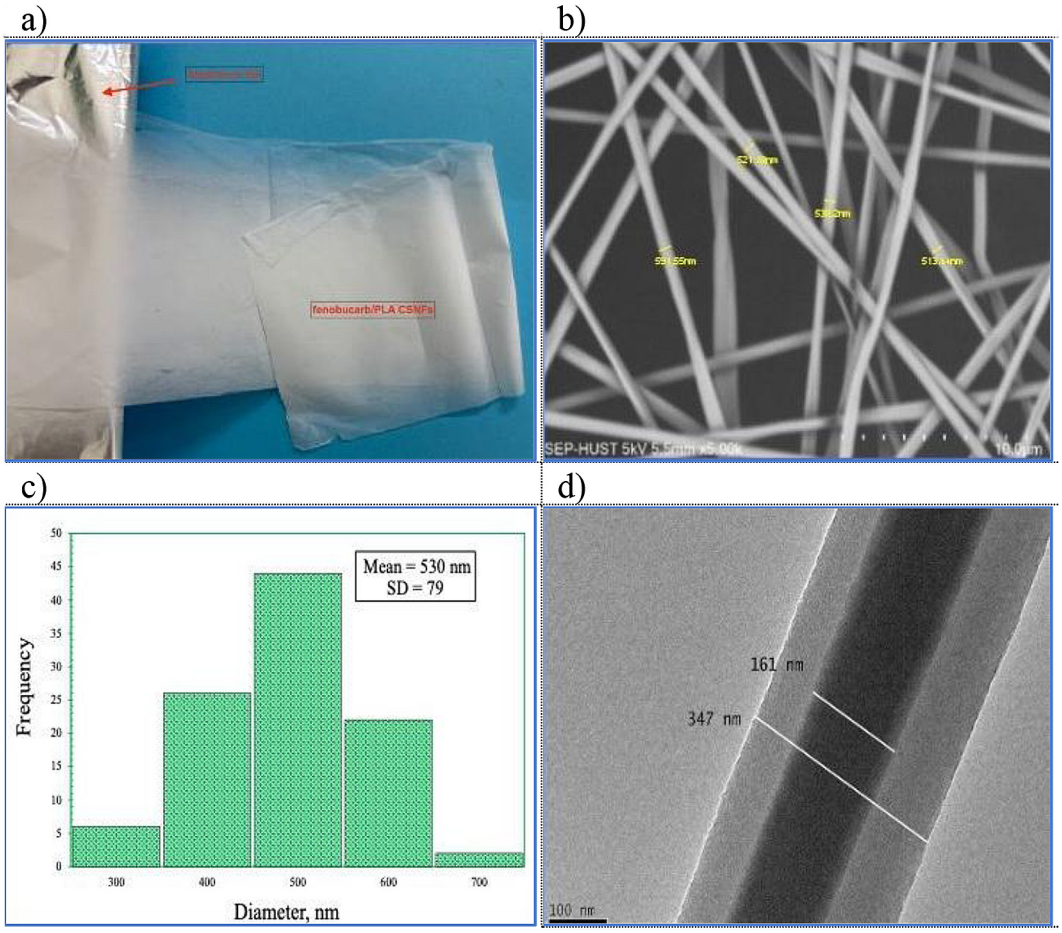

Figure 3. CSNFs scaffold structure (a), SEM micrograph (b), nanofiber diameter distribution (c), and TEM image of CSNFs (d)

The use of toluene as the core solvent introduces additional instability due to its low polarity and limited compatibility with DMF. This mismatch can disturb the integrity of the core shell interface, leading to fluctuations in the coaxial jet and contributing to fiber twisting and variation in diameter. In addition, the relatively low concentrations of fenobucarb and PLA, both at 10 wt%, reduce chain entanglement and lower the viscoelastic properties of the solution, which further destabilizes the jet. As a result, the produced fibers exhibit non cylindrical shapes, uneven diameter distribution, and structural deformation.

The TEM image (Figure 3d) clearly shows a well-defined core shell structure, confirming successful formation of coaxial nanofibers. A darker central region and a lighter outer layer are visible, corresponding to the fenobucarb core and PLA shell. This contrast is due to the higher electron density of the core material compared to the polymer shell. Measurements indicate a core diameter of approximately 161 nm and an overall fiber diameter of about 347 nm, which suggests a relatively uniform shell thickness along the fiber axis. This observation reflects stable coaxial jet formation during the electrospinning process. The core appears well centered within the fibers, which suggests that the flow rates of the core and shell solutions were properly balanced during electrospinning. Any slight asymmetry observed may result from interfacial instability caused by the limited compatibility between toluene in the core and the DMF containing shell solution.

In vitro fenobucarb release behavior and kinetics

The fenobucarb loading in the prepared nanofibers was first quantified, followed by evaluation of its release behavior over time. Gas chromatography was employed to determine the fenobucarb content in the CSNFs, and the results calculated from Equation 1 are presented in Figure 4. The release profile was then determined by calculating the amount of fenobucarb released as a function of time using Equation 2, with the corresponding data shown in Figure 5 and Table 4.

As presented in Figure 4, the fenobucarb loading in the CSNFs reached 17.976%. Under the applied electrospinning conditions and selected solution compositions, the theoretical loading could reach approximately 23.077%. The lower experimental value is likely due to partial loss of fenobucarb during fiber formation, which occurs as a result of solvent evaporation in the electrospinning process.

The data in Figure 5a indicate that fenobucarb/PLA nanofiber scaffolds provide a sustained release profile. During the first two days, the release rate remains low, reaching about 6.24%, which reflects an initial lag phase. This behavior is attributed to the hydrophobic nature of the PLA shell, which delays water penetration. Once the scaffold becomes sufficiently wetted, the release rate increases. The cumulative release reaches approximately 17.78% after 5 days and 33.23% after 10 days. The release accelerates

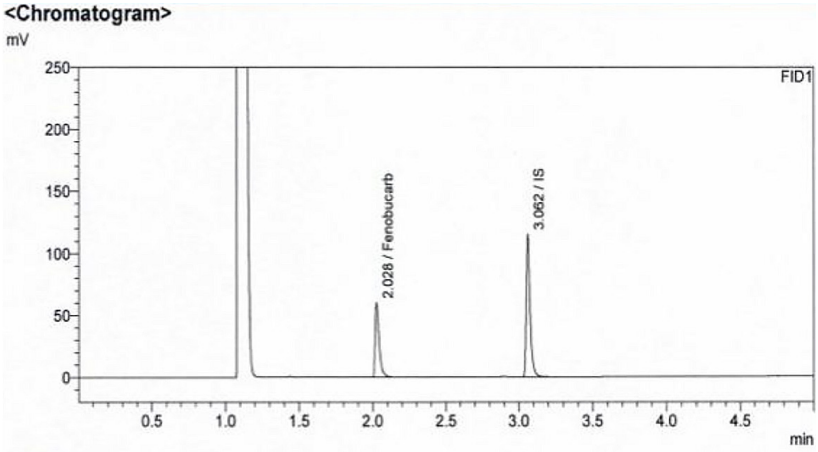

<Peak Table>

FID1

Peak#	Ret. Time	Area	Height	Conc.	Unit	Mark	Name
1	2.028	113102	59228	17.976	%		Fenobucarb
2	3.062	208740	113270	0.000	%	S	IS
Total		321842	172498				

Figure 4. Fenobucarb loaded content in CSNFs

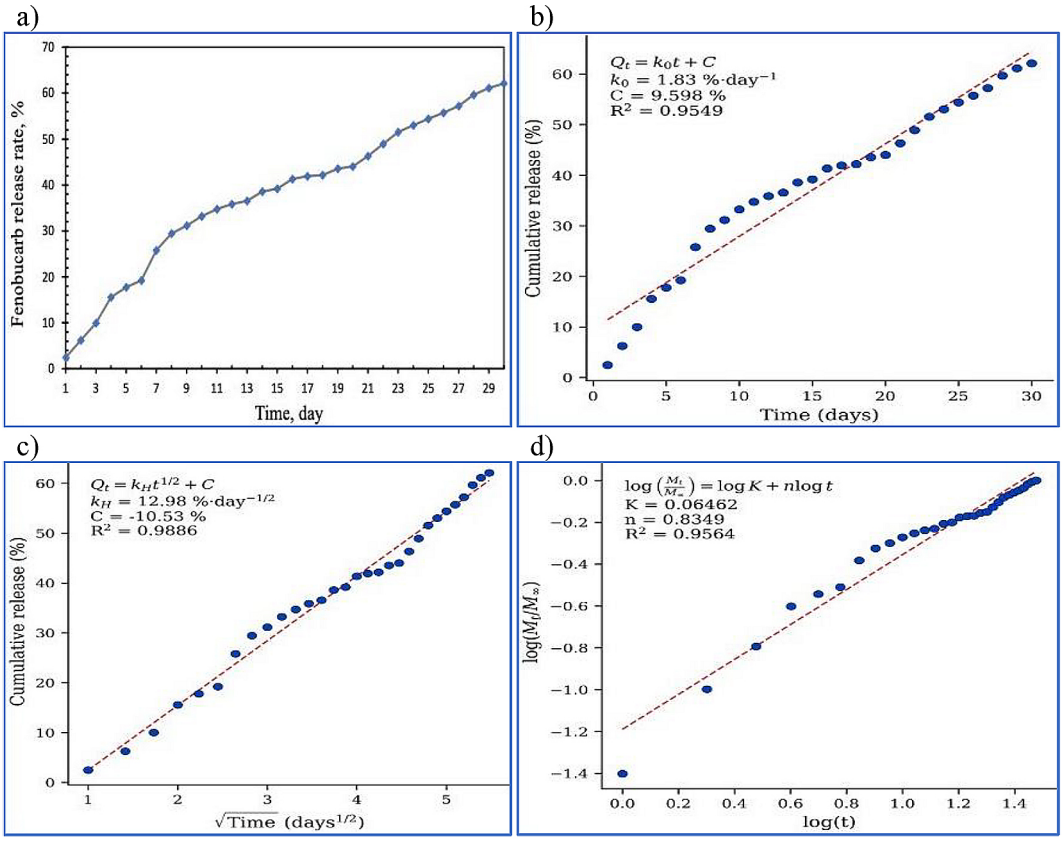

Figure 5. Fenobucarb release rate (a), Fenobucarb released Zero-order (b), Higuchi (c), Korsmeyer-Peppas kinetic models (d)

Table 4. Kinetic parameters obtained by fitting fenobucarb release data to different models

Model	Zero-order	Higuchi	Korsmeyer-Peppas
Fenobucarb nanofiber scaffold	K_0 = 1.83%.day^{-1} R^2 = 0.9549 Adjusted R^2 = 0.9533 RMSE = 3.4402	k_H = 12.98%. day$^{-1/2}$ R^2 = 0.9886 Adjusted R^2 = 0.9882 RMSE = 1.7331	K = 0.06462 R^2 = 0.9564 Adjusted R^2 = 0.9548 RMSE = 0.0648

Note: The RMSE of the Korsmeyer-Peppas model was calculated on the log-transformed scale and should not be directly compared with RMSE values from the zero-order and Higuchi models.

between day 2 and day 10, then gradually decreases. From day 20 to day 30, the release profile becomes more stable.

In order to clarify the release mechanism, the experimental release data were fitted to zero-order, Higuchi, and Korsmeyer-Peppas kinetic models. Model fitting was evaluated using R^2, adjusted R^2, and RMSE. The zero-order model showed a relatively good fit, with R^2 = 0.9549, adjusted R^2 = 0.9533, and root mean square error (RMSE) = 3.4402. The calculated zero-order release constant was k_0 = 1.83 %·day^{-1}, indicating a moderate average release rate over the tested period. However, the higher RMSE and visible deviations from the fitted line, especially at early time points, indicate that fenobucarb release did not follow ideal zero-order kinetics throughout the full release period.

The Higuchi model provided the best fit among the tested models, with the highest R^2 = 0.9886 and adjusted R^2 = 0.9882, together with the lowest RMSE = 1.7331. The strong linear relationship between cumulative release and the square root of time indicates that fenobucarb release was mainly governed by diffusion through the PLA matrix. The Higuchi constant, kH = 12.98 %·day$^{-1/2}$, further supports a diffusion controlled release process. Compared with the zero-order model, the lower fitting error of the Higuchi model shows that diffusion better

explains the release behavior of fenobucarb from the core-shell nanofiber scaffold.

The Korsmeyer–Peppas model also showed a good fit, with R^2 = 0.9564, adjusted R^2 = 0.9548, and RMSE = 0.0648 on the logarithmic scale. The release exponent n = 0.8349 indicates anomalous transport, suggesting that the release mechanism involved both diffusion and polymer relaxation. However, its adjusted R^2 was lower than that of the Higuchi model. In addition, the RMSE value for the Korsmeyer–Peppas model was calculated on the log-transformed scale, so it should not be directly compared with the RMSE values of the zero-order and Higuchi models, which were calculated from cumulative release percentages.

Overall, the kinetic evaluation indicates that the release of fenobucarb from the fenobucarb/PLA core-shell nanofiber scaffold was mainly diffusion-controlled, as demonstrated by the superior fitting performance of the Higuchi model. The Korsmeyer-Peppas exponent suggests that polymer relaxation may also contribute to the release process, but diffusion through the PLA shell appears to be the dominant mechanism. The zero-order model captured the general release trend but did not fully describe the release profile across the full experimental period. The proposed mechanism of fenobucarb release from the fenobucarb/PLA nanofiber scaffold is illustrated in Figure 6.

The release behavior of fenobucarb from fenobucarb/polylactic acid core shell nanofiber scaffolds is illustrated in Figure 6. Because PLA is hydrophobic and degrades slowly in aqueous environments, the release process is mainly controlled by diffusion through the polymer matrix and by fiber wettability. In general, fenobucarb release from PLA based nanofibers involves surface desorption, diffusion, and gradual polymer degradation. For this system, where both fenobucarb and PLA are hydrophobic, the release process can be divided into five stages.

First, water from the surrounding medium slowly contacts the fiber surface and dissolves a small amount of fenobucarb located near the outer layer. This step proceeds slowly due to the hydrophobic nature of both components, which leads to an initial lag phase. Second, water begins to penetrate into the PLA shell through free volume and micro pores. This allows additional fenobucarb to dissolve and start diffusing outward. Third, once sufficient hydration is achieved, the release is dominated by diffusion through the PLA shell, driven by the concentration gradient between the core and the external medium. Fourth, as the amount of fenobucarb in the core decreases, the diffusion pathway becomes longer and the concentration gradient weakens. This leads to a gradual reduction in the release rate. Finally, in the later stage, the PLA shell undergoes slow degradation and erosion, forming pores and microcracks. These structural changes facilitate the continued release of the remaining fenobucarb, where the mechanism involves both diffusion and polymer relaxation or degradation.

Preliminary field performance assessment

For comparison, the commercial formulation Dibacide 50 EC was used as a reference, while a water treated plot served as the control. Liquid treatments were applied by uniformly spraying the crop canopy using 18 L electric backpack sprayers. No additional plant protection products were used during the experiment to avoid interference. Efficacy was evaluated at ten sampling points arranged along two diagonal transects within each plot. To reduce edge effects, each point was located at least 1 m from the plot boundary. Aphid density was determined as the average number of aphids per plant across all sampling points.

To establish accurate application rates, the actual fenobucarb content in the WP and SC formulations was quantified using gas

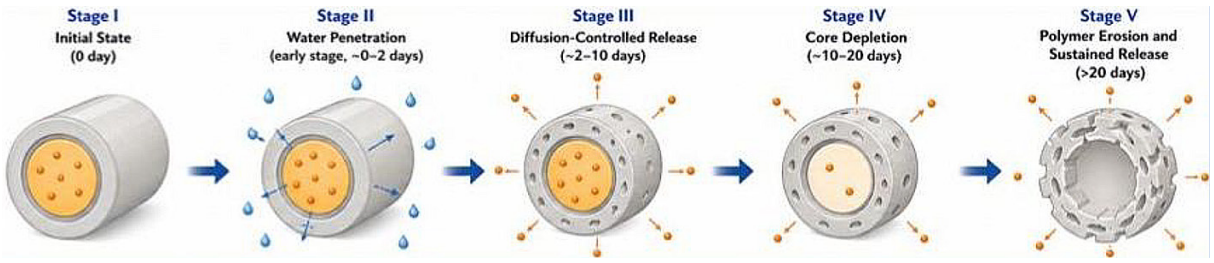

Figure 6. Proposed mechanism of fenobucarb release from CSNFs scaffolds

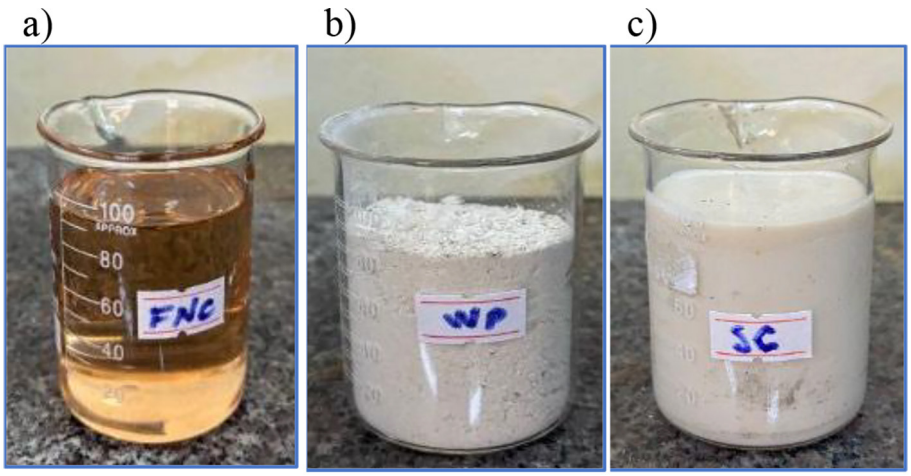

Figure 7. Neat fenobucarb (a), WP nano CSNFs (b), SC nano CSNFs (c)

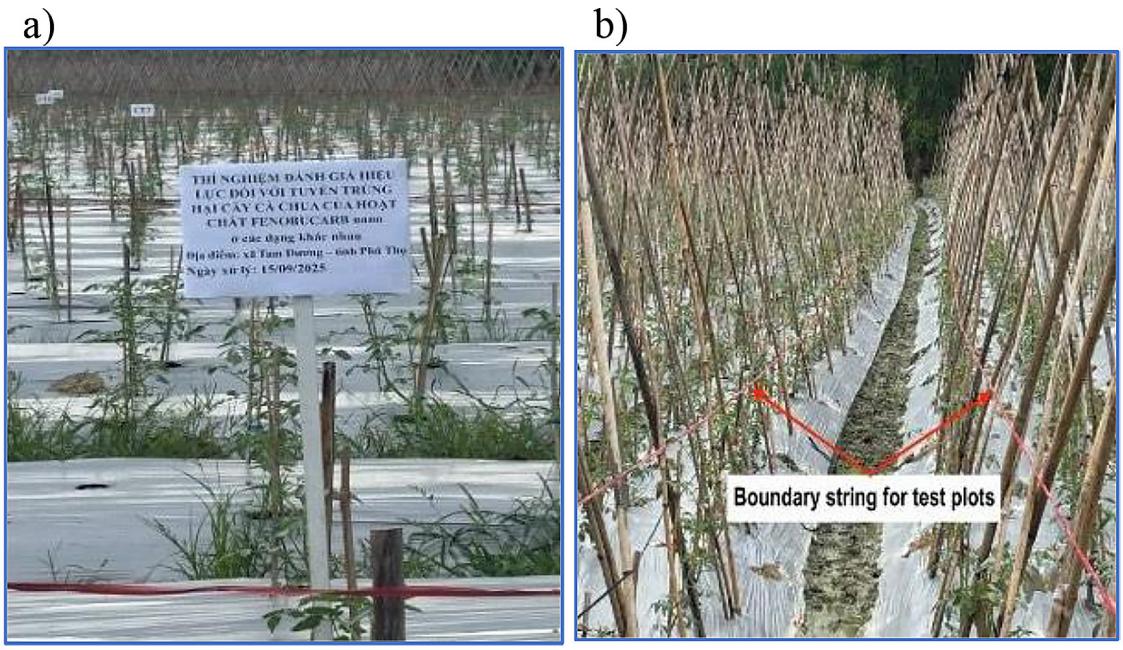

Figure 8. Tomato plots used for the preliminary field efficacy assessment

chromatography with a flame ionization detector. Both formulations showed a fenobucarb content of 5.26% (Figure 7). The slight deviation from the theoretical value of 5.39% is attributed to losses during processing and residual solvent present in the nanofibers. Based on these measured values and the national standard requirement of 250 g of fenobucarb per hectare, the application rates for each treatment were calculated, as summarized in Table 5.

Table 5. Treatment conditions

No.	Treatments	Dose/ha		Dilution in water/ha
		Technical g a.i./ha	g formulation/ha	
1	WP product	250	4752.9	500 L
2	SC product	250	4752.9	500 L
3	Dibacide 50EC	500	1000	500 L
4	Untreated	0	0	0

The efficacy results for fenobucarb loaded nanofiber formulations and their effects on tomato plants at different time points are summarized in Tables 6 to Table 8. Treatments were applied to tomato crops, and evaluations began immediately after application, with observations conducted at five days intervals. Plant response was assessed using a phytotoxicity scale from level 1, indicating no visible damage, to level 9, indicating complete plant death.

At all observation times, tomato plants treated with the WP, SC, and the reference formulation Dibacide 50 EC showed no signs of phytotoxicity. These observations indicate that both WP and SC formulations caused no visible phytotoxicity to tomato plants under the tested conditions (Figure 8).

To assess the effectiveness of the fenobucarb nano formulations (WP and SC) against aphids, field surveys were conducted at regular intervals to monitor aphid survival. Aphid density was calculated as the number of live aphids divided by the total number of plants examined. The results, which reflect changes in aphid population under each treatment, are presented in Tables 7 and Table 8.

The descriptive data in Table 7 indicate a reduction in aphid populations following treatment with the SC and WP formulations. After 30 days, aphid density decreased from 10.8 to 4.1 aphids per leaf for SC, and from 7.3 to 5.2 aphids per leaf for WP. All treatments, including WP, SC, and the reference Dibacide 50 EC, maintained a phytotoxicity level of 1 throughout the study, indicating no visible damage to tomato plants under field conditions.

In the untreated control, aphid density increased sharply from 8.5 to 31.8 aphids per leaf at 30 days, which confirms favorable conditions for pest growth in the absence of control. In contrast, both nano formulations suppressed

Table 6. Phytotoxicity observations of tomato plants after treatment application

No.	Treatments	Toxicity level						
		DBT	5 DAT	10 DAT	15 DAT	20 DAT	25 DAT	30 DAT
1	WP product	1	1	1	1	1	1	1
2	SC product	1	1	1	1	1	1	1
3	Dibacide 50EC	1	1	1	1	1	1	1
4	Untreated	1	1	1	1	1	1	1

Note: DBT refers to days before treatment, and DAT indicates days after treatment.

Table 7. Descriptive aphid density data during the preliminary field assessment

No.	Treatments	Density, aphids/leaf						
		DBT	5 DAT	10 DAT	15 DAT	20 DAT	25 DAT	30 DAT
1	WP product	7.3	6.5	7.1	6.8	6.4	6.0	5.2
2	SC product	10.8	9.7	9.4	8.5	6.7	6.0	4.1
3	Dibacide 50EC	9.5	9.1	8.6	10.2	10.7	10.9	12.5
4	Untreated	8.5	11.7	13.9	16.0	18.5	25.2	31.8

Note: Values are descriptive mean aphid densities from ten within-plot sampling points. Because individual sampling-point values were not retained, SD values are not reported. These data were not used for inferential statistical comparison.

Table 8. Descriptive efficacy of fenobucarb treatments calculated using the Henderson-Tilton formula

No.	Treatments	Effectiveness of the CSNFs, E (%)					
		5 DAT	10 DAT	15 DAT	20 DAT	25 DAT	30 DAT
1	WP product	35.6	40.5	50.5	59.9	72.3	81.0
2	SC product	35.2	46.7	58.2	71.6	81.3	89.9
3	Dibacide 50EC	30.5	44.6	42.9	48.3	64.1	64.8

aphid populations over time. The WP treatment showed a minor fluctuation at 10 days, followed by a gradual decrease, indicating stable but moderate control. The SC formulation showed a more consistent decline, which indicates stronger and longer lasting activity.

The Dibacide 50 EC treatment reduced aphid density at early stages but failed to maintain control, with populations rising to 12.5 aphids per leaf after 30 days. This pattern indicates limited residual effectiveness. The calculated efficacy values support these observations. The SC formulation reached 89.9 percent at 30 days, while WP achieved 81.0 percent. Dibacide 50 EC remained below 65 percent and showed less stable performance.

Overall, the preliminary field data suggest that the nanofiber-based formulations, especially the SC type, maintained aphid suppression over the observation period without visible phytotoxic effects under the tested conditions. A limitation of this preliminary field assessment is the absence of replicated randomized plots. Therefore, the field data do not allow inferential statistical comparison or confirmation of treatment superiority. Differences in initial aphid density among plots may also affect treatment comparability. The results should therefore be considered as initial field evidence supporting further evaluation of the formulations in replicated randomized trials.

CONCLUSIONS

This study showed that fenobucarb-loaded PLA core-shell nanofibers were prepared by coaxial electrospinning. SEM analysis showed nanofibers with diameters ranging from 200 to 800 nm, with an average diameter of approximately 530 ± 79 nm. TEM observation confirmed the formation of a distinct core-shell structure, indicating that fenobucarb was incorporated within the PLA-based nanofiber system. The fenobucarb loading content reached 17.976%, indicating effective incorporation of the active ingredient into the nanofiber scaffold. The in vitro release profile showed sustained fenobucarb release over 30 days, with an initial lag phase followed by a diffusion controlled stage. Among the tested kinetic models, the Higuchi model gave the best fit, with $R^2 = 0.9886$, adjusted $R^2 = 0.9882$, and RMSE = 1.7331. This result supports the hypothesis that the PLA shell delayed fenobucarb diffusion and acted as a release-controlling barrier. The Korsmeyer-Peppas model further suggested that polymer relaxation also contributed to the release process.

The preliminary field assessment indicated that the wettable powder and suspension concentrate formulations reduced aphid density on tomato plants under the tested cultivation conditions. The descriptive efficacy values at 30 days after treatment were 81.0% for the wettable powder formulation and 89.9% for the suspension concentrate formulation. No visible phytotoxic symptoms were observed in tomato plants during the assessment period. However, because the field assessment did not include replicated randomized plots, these results should be interpreted as preliminary field evidence rather than statistically confirmed treatment superiority.

The main scientific contribution of this study is the demonstration of a fenobucarb-loaded PLA core-shell nanofiber system that combines coaxial electrospinning, sustained release behavior, and conversion into practical pesticide formulation types. The findings partially support the proposed hypothesis by showing sustained release and preliminary aphid suppression without visible phytotoxicity. Further work should include replicated randomized field trials, full statistical validation, batch-to-batch reproducibility assessment, long-term stability testing, environmental fate analysis, and evaluation under different crop and pest conditions.

Acknowledgements

The authors would like to sincerely thank the Functional Polymer Laboratory - HUST for providing measurement equipment support for this research, Mr. Tao Minh Tuan (Center for Research and Consulting on the Development of Plant Protection Drugs and Fertilizers) for their assistance in preparing the pesticide and conducting field trials.

REFERENCES

1. Ahmad M.F., Ahmad F.A., Alsayegh A.A., Zeyaullah M., AlShahrani A.M., Muzammil K., Saati A.A., Wahab S., Elbendary E.Y., Kambal N., Abdelrahman M.H., Hussain S. (2024). Pesticides impact on human health and the environment with their mechanisms of action and possible countermeasures. *Heliyon*, *10*(7), e29128. https://doi.org/10.1016/j.heliyon.2024.e2912

2. Zanino A., Pizzetti F., Masi M., Rossi F. (2024). Polymers as controlled delivery systems in agriculture: The case of atrazine and other pesticides. *European Polymer Journal*, *203*, 112665. https://doi.org/10.1016/j.eurpolymj.2023.112665
3. Alli Y.A., et al. (2024). Coaxial electrospinning: design, characterization, and applications of core–shell nanofibers. *Journal of Materials Science & Technology*, *176*, 1–20. https://doi.org/10.1016/j.jmst.2023.10.045
4. Bishnoi A., Tiwari R.K., Chanda S., Ajmal G., Bonde G.V. (2023). Elecrospun nanofibers: The versatile platform as a drug delivery system in healthcare. *Journal of Drug Delivery Science and Technology*, *90*, 105127. https://doi.org/10.1016/j.jddst.2023.105127
5. Carvalho, F.P. (2017). Pesticides, environment, and food safety. *Annual Review of Environment and Resources, 42*, 215–239. https://doi.org/10.1146/annurev-environ-102016-060551
6. Chawda D., and Ninave S. (2021). Farmers' exposure to pesticides – A review. *Journal of Pharmaceutical Research International*, *33*(60B), 3085–89. https://doi.org/10.9734/jpri/2021/v33i60B34981
7. Chen H., Zhang W., Wang Y., Liu X., Li J., Zhao C. (2021). Development of leaf-adhesive pesticide nano capsules with pH-responsive release to enhance retention time on crop leaves. *Journal of Materials Chemistry B, 9*(3), 629–638. https://doi.org/10.1039/D0TB02430A
8. Doan V.A., Anh L.T.H., Phung T.A., Vu D.M., Khac V.T., Nguyen L.T. (2025). Controlled-release pesticide nanofibers for sustainable agriculture: effects of processing parameters on fiber morphology and release kinetics. *Journal of ecological engineering, 26*(6), 48–61. https://doi.org/10.12911/22998993/201995
9. Doan V.A., Anh L.T.H., Vu V.V., Khac V.T., Nguyen L.T. (2025). PBAT/PLA nanofibers prepared via coaxial electrospinning: The effect of core feed rate on the nanofibers characteristics. *Egyptian Journal of Chemistry, 68*(6), 369–380. https://doi.org/10.21608/ejchem.2024.316810.10304
10. Elhamalawy O., et al. (2024). Impact of pesticides on non-target invertebrates in agricultural ecosystems. *Pesticide Biochemistry and Physiology, 197*, 105974. https://doi.org/10.1016/j.pestbp.2024.105974
11. Gaydhane M.K., Sharma C.S., Majumdar S. (2023). Electrospun nanofibers in drug delivery: Advances in controlled release strategies. *RSC Advances, 13*(11), 7312–7328. https://doi.org/10.1039/D2RA06023J
12. Wu H., Li Z. (2022). Recent advances in nano-enabled agriculture for improving plant performance. *The Crop Journal, 10*(1), 1–12. https://doi.org/10.1016/j.cj.2021.06.002
13. Shi H., Guo Y., Dong Z. (2026). Controlled release system of pesticide nanoparticles based on intelligent response: current status and development trend. *Pesticide Biochemistry and Physiology*, *216*(1), 106710. https://doi.org/10.1016/j.pestbp.2025.106710
14. Huang. (2025) Pesticide reduction, climate change, and food security: evidence from rice production in China. *Frontiers in Sustainable Food Systems*, https://doi.org/10.3389/fsufs.2025.1669981
15. Xiong H., Duan J., Cao W., Su Y., Chen H., Zhao P., Wang Z., Wang J., Lu H., and Yu K. (2025). Nanoemulsion as the pioneer carrier for future green nanopesticides. *Langmuir*, *41*(30), 19625–19641. https://doi.org/10.1021/acs.langmuir.5c02340
16. Khan J., Khan A., Khan M.Q., Khan H. (2024). Applications of co-axial electrospinning in the biomedical field. *Next Materials, 3*, 100138. https://doi.org/10.1016/j.nxmate.2024.100138
17. Kah M., Hofmann T., Keller A.A. (2019). Nano-enabled pesticides for sustainable agriculture and global food security. *Nature Nanotechnology, 14*(6), 532–540. https://doi.org/10.1038/s41578-019-0124-6
18. Kalluri H., Choi J., Kim H. (2021). Effect of electrospinning parameters on the fiber diameter of PLGA nanofibers. *Materials, 14*(7), 1626. https://doi.org/10.3390/ma14071626
19. Khan J., Ali S., Ahmed N., Rehman A. (2024). Applications of co-axial electrospinning in the biomedical field: Fabrication, structure, and performance of core-shell nanofibers. *Results in Engineering, 21*, 101621. https://doi.org/10.1016/j.rineng.2024.101621
20. Le L.T., Nguyen H.T., Nguyen L.T., Tran H.Q., Nguyen T.T.T. (2024). Berberine-loaded polylactic acid nanofiber scaffold as a drug delivery system: The relationship between chemical characteristics, drug-release behavior, and antibacterial efficiency. *Beilstein Journal of Nanotechnology, 15*, 71–82. https://doi.org/10.3762/bjnano.15.7
21. Liu J., Wang Y., Chang J., Zhao S., Salam A., Zhu S., Ou G., Zhang P., Zhang Z. (2025). Laccase-responsive biobased nanocarriers from lignin/chitosan for enhanced foliar adhesion and targeted pesticide delivery. *ACS Sustainable Chemistry & Engineering, 13*(42), 18188–18201. https://doi.org/10.1021/acssuschemeng.5c07904
22. Majumder R. (2024). Balancing food security and environmental safety: rethinking modern agricultural practices. *Environmental and Experimental Biology, 21*(4), 101–110. https://doi.org/10.22364/eeb.21.12
23. Nguyen L.T., Doan V.A., Phung T.A. (2026). Slow-release fenobucarb nanofibers: a case study

on field efficacy against brown planthopper in rice cultivation in Vietnam. *Journal of Ecological Engineering, 27*(2), 345–356. https://doi.org/10.12911/22998993/211657

24. Nguyen L.T., Doan V.A., Phung T.A. (2026). Sustained-release profenofos encapsulated polylactic acid nanofibers: evaluation in maize cultivation under actual field conditions. *Journal of Ecological Engineering, 27*(4), 179–192. https://doi.org/10.12911/22998993/214962
25. Nguyen T.M., Le N.T.T., Havukainen J., Hannaway D.B. (2018). Pesticide use in vegetable production: A survey of Vietnamese farmers' knowledge. *Plant Protection Science, 54*, 203–214. https://doi.org/10.17221/96/2017-PPS
26. Fabiyi O.A., Ogundele A.V., Mella H.S. (2025). Polysaccharide polymer-based nanoparticles for nano fertilizer and nano pesticides: A review. *Carbohydrate Polymer Technologies and Applications, 12*, 101009. https://doi.org/10.1016/j.carpta.2025.101009
27. Raksa P., Srichana T., Tippayawong N. (2021). Effect of humidity on the characteristics of electrospun nanofibers. *Heliyon, 7*(12), e08491. https://doi.org/10.1016/j.heliyon.2021.e08491
28. Zainab R., Hasnain M., Ali F., Abideen Z., Siddiqui Z.S., Jamil F., Hussain M., Park Y.-K. (2024). Prospects and challenges of nanopesticides in advancing pest management for sustainable agricultural and environmental service. *Environmental Research, 261*, 119722. https://doi.org/10.1016/j.envres.2024.119722
29. Viter R., Iatsunskyi I., Nowaczyk G., Jurga S. (2025). Novel core-shell nanofibers fabricated by coaxial electrospinning for advanced functional applications. *Nanomaterials, 15*(13), 1026. https://doi.org/10.3390/nano15131026
30. Wang Y., Tang Z., Tabusibieke C., Gao H., Lu W. (2026). Nanopesticides by design: A review of delivery platforms, environmental fate, and standards for safe and sustainable crop protection. *Molecules, 31*(3), 453. https://doi.org/10.3390/molecules31030453
31. Xin X., Judy J.D., Sumerlin B.B., He Z. (2020). Nano-enabled agriculture: from nanoparticles to smart nanodelivery systems. *Environmental Chemistry 17*, 413–425. https://doi.org/10.1071/EN19254
32. Yu D.G., Li J.J., Williams G.R. (2023). Coaxial electrospinning: fundamentals and applications for drug delivery. *Advanced Fiber Materials, 5*(2), 189–212. https://doi.org/10.1007/s42765-022-00184-5
33. Zhao X., Cui H., Wang Y., Sun C., Cui B. (2023). Development strategies and prospects of nano-based smart pesticide formulation. *International Journal of Molecular Sciences, 24*(3), 2403. https://doi.org/10.3390/ijms24032403
34. Zhou W., Li M., Achal V. (2025). A comprehensive review on environmental and human health impacts of chemical pesticide usage. *Emerging Contaminants, 11*(1), 100410. https://doi.org/10.1016/j.emcon.2024.100410